Thermal Properties and Morphology of a Poly(vinyl alcohol)/Silica Nanocomposite Prepared with a Self-Assembled Monolayer Technique

Zheng Peng,[1] Ling Xue Kong,[1] Si-Dong Li[2]

[1]*Centre for Advanced Manufacturing Research, University of South Australia, Mawson Lakes SA 5095, Australia*
[2]*College of Science, Zhanjiang Ocean University, Zhanjiang 524088, People's Republic of China*

Received 10 September 2003; accepted 2 December 2004
DOI 10.1002/app.21583
Published online in Wiley InterScience (www.interscience.wiley.com).

ABSTRACT: A poly(vinyl alcohol) (PVA)/silica (SiO_2) nanocomposite was prepared with a novel self-assembled monolayer technique, and its morphology and thermal properties were studied with different material characterization instruments. The treated SiO_2 nanoparticles were dispersed in the PVA matrix homogeneously, and the thermal properties of the nanocomposite were markedly improved in comparison with those of pure PVA. Under the same isothermal heating conditions, the decomposition of the nanocomposite was delayed significantly in comparison with that of PVA. The thermal degradation of the nanocomposite was a two-step reaction, including the degradation of the side chain and main chain. The products of side-chain degradation were mainly carboxylic acid, whereas main-chain degradation primarily produced carbon dioxide and low-molecular-weight conjugated polyene. © 2005 Wiley Periodicals, Inc. J Appl Polym Sci 96: 1436–1442, 2005

Key words: monolayers; morphology; nanocomposites; self-assembly; silicas; thermal properties

INTRODUCTION

In recent years, polymer-based nanocomposites have attracted more and more attention because nanoparticles have significant surface effects, size effects, and quantum effects that improve material properties, including toughness and stiffness, transparency, scratch, abrasion, solvent, and heat resistance, and gas permeability. They have been used for medical applications, coatings, fillers, and conductive polymers.[1–5]

Poly(vinyl alcohol) (PVA), having water-soluble, biodegradable, biocompatible, gas-barrier, and high mechanical properties, is attractive for environmentally friendly products, medical applications, protein purification, enzyme immobilization, and membrane preparation.[6–14] More recently, PVA-based nanocomposites have been developed to improve PVA's properties and further explore its applications.[15–17] Most PVA-based nanocomposites are prepared with the sol–gel method.

The key issue for preparing a polymeric–inorganic nanocomposite is the dispersion of inorganic nanoparticles in a polymer matrix uniformly while aggregation is avoided. To solve this problem, various processes have been developed. Widely used methods for synthesizing polymeric–inorganic nanocomposites included sol–gel, *in situ* polymerization, intercalation polymerization, and blending techniques. The layer-by-layer self-assembled monolayer (SAM) technique, introduced by Decher and Hong in 1991,[18] has received increasing attention in recent years. This technique is based on the electrostatic attractive interaction of oppositely charged polyelectrolytes. Although the driving forces in the SAM technique are dominated by electrostatic attractive interactions between positive and negative charges, other interactions, such as hydrophobic interactions, charge-transfer interactions, π–π stacking forces, hydrogen bonding, coordination bonding, and covalent bonding, have also been used successfully.[19–23] Negatively charged silica (SiO_2) nanoparticles have been reported as materials used for fabricating SAM ultrathin films.[24,25]

Although the SAM technique had previously just been used to construct ultrathin multiplayer films, it was employed here to prepare bulk PVA/SiO_2 nanocomposites. Scanning electron microscopy (SEM) with energy-dispersive X-ray detection, transmission electron microscopy (TEM), and Fourier transform infrared (FTIR) spectroscopy were used to investigate the interactions and morphology of the prepared nanocomposite, whereas thermogravimetric analysis (TGA) was employed to analyze its thermal stability. Its glass-transition temperature (T_g) was studied with differential scanning calorimetry (DSC), and the thermal degradation process was analyzed with a combined FTIR/TGA system.

Correspondence to: L. X. Kong (lingxue.kong@unisa.edu.au).

© 2005 Wiley Periodicals, Inc.

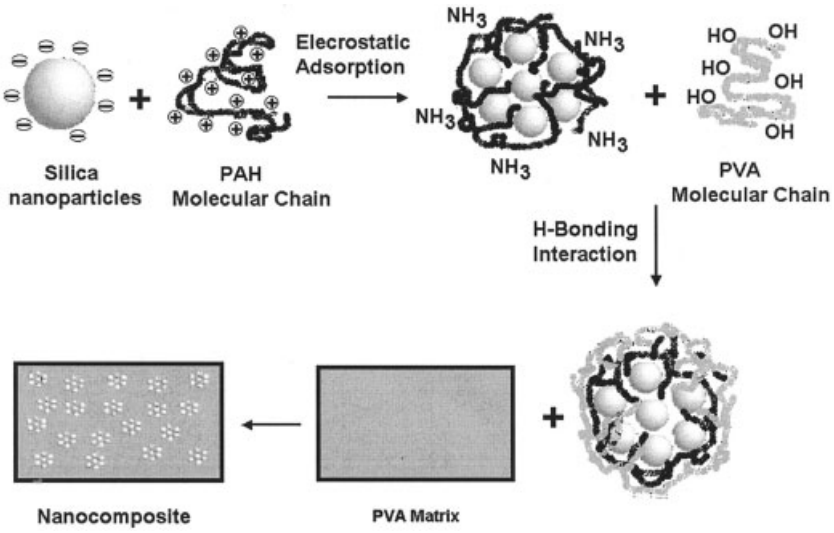

Figure 1 Scheme of the SAM nanocomposite process.

EXPERIMENTAL

Materials

All materials used in this work, including PVA, SiO_2 nanoparticles, and poly(allylamine hydrochloride) (PAH), were acquired from Sigma–Aldrich (Sigma-Aldrich, St. Louis, MO). The average molecular weight of PVA was approximately 67,000, the degree of polymerization was 1400, and the degree of hydrolysis was 86.7–88.7 mol %. The SiO_2 nanoparticles had an average diameter of 14 nm and a surface area of 200 $\pm$ 25 m^2/g. PAH had an average molecular weight of 70,000. The water was Milli-Q water (18 MΩ cm). All materials were used as received.

Preparation of the PVA/SiO_2 nanocomposite

A scheme for preparing the PVA/SiO_2 nanocomposite is presented in Figure 1. Positively charged PAH molecular chains were adsorbed onto the surface of negatively charged SiO_2 nanoparticles through electrostatic adsorptive interactions. Afterwards, PVA molecular chains were attracted to the surface of the SiO_2 nanoparticles through hydrogen-bonding interactions between the hydroxy groups of PVA and the amido groups of PAH. Finally, the SiO_2 nanoparticles were well dispersed in the PVA matrix. In comparison with other methods, this SAM method has many significant advantages. It is simple and can be performed at a low cost but with uniform dispersion. It is only suitable for hydrophilic polymers.

The nanocomposite (PVA/SiO_2 = 95/5 w/w) was prepared according to the following procedure. A 1 wt % SiO_2 nanoparticle aqueous dispersion (100 mL) was treated with an ultrasonic vibrator for 0.5 h, and its pH was then adjusted to 10 with 0.2 M NaOH. A 0.5 wt % positively charged PAH solution (50 mL) was dropped into the SiO_2 dispersion, which was mechanically stirred simultaneously.

The dispersion was centrifuged and rinsed to remove PAH that was not absorbed onto the surface of the SiO_2 nanoparticles, and this step was repeated three times. Afterwards, a 0.5 wt % 50-mL PVA solution was dropped into the rinsed SiO_2 dispersion, which was mechanically stirred for 1 h to produce a stable SiO_2 dispersion. This dispersion was dropped into a 20 wt % 100-mL PVA solution with mechanical stirring for about 5 h at room temperature to produce a homogeneous PVA/SiO_2 nanocomposite, which was cast into a polytetrafluorethylene Petri dish and dried in a vacuum oven at 50°C for 1 week to produce a nanocomposite film.

Measurements

The SEM micrographs were taken with a Philips XL30-EDAX instrument (Philips, Eindhoven, The Netherlands) with an energy-dispersive X-ray detector. The fracture surface was obtained by the splitting of a bulk sample quenched in liquid nitrogen. A sputter coater was used to precoat conductive gold onto the fracture surface before the microstructure was observed. A thin film for TEM was prepared by the nanocomposite solution, diluted 10 times with water, being dropped onto a copper grid coated with a carbon film. TEM measurements were performed with a JEM-100CXII instrument (JEOL, Peabody, MA) at an accelerating voltage of 100 kV.

DSC analysis was performed on a PerkinElmer Pyris 1 system (Perkin-Elmer, Fremont, CA) under a nitrogen flow, which was calibrated with indium. A sample weighing between 10 and 12 mg was annealed at 110°C for 10 min, quenched in liquid nitrogen, and scanned up to 220°C at a heating rate of 10°C/min. T_g

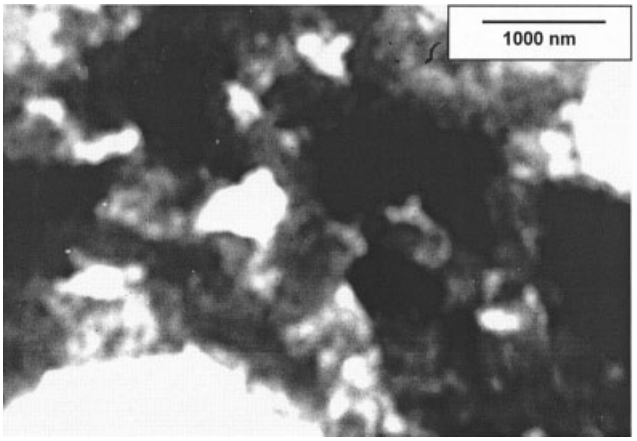

Figure 2 Micrograph of the dispersion of untreated SiO_2 nanoparticles (TEM).

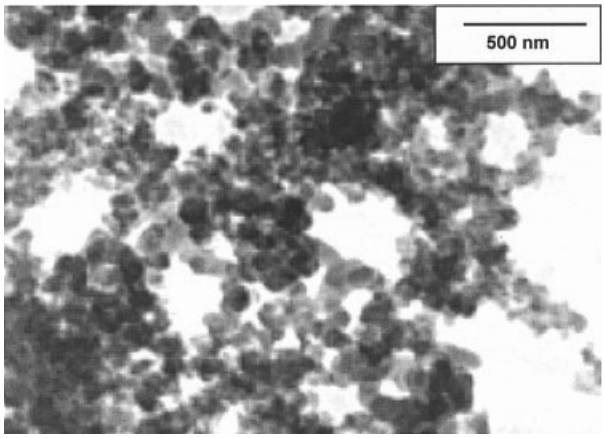

Figure 4 Micrograph of the PVA/SiO_2 nanocomposite (TEM).

was taken as the half-peak of the corresponding heat capacity jump, and the melting temperature (T_m) was measured as the melting peak of the DSC trace.

A PerkinElmer TGA-7 thermogravimetric analyzer was used for the thermal decomposition measurements. The measurement of the films (ca. 10 mg) was carried out from 100 to 600°C at a heating rate of 20°C/min under a nitrogen atmosphere at a flowing rate of 80 mL/min.

The thermal degradation was characterized online with a combined FTIR/TGA system. To eliminate the interference of gases that evolved during the different degradation steps, the nanocomposite was continuously heated at three temperatures. First, the nanocomposite was heated at 110°C for 10 min to eliminate the water; it was then heated at the temperature of the maximum weight-loss rate (T_p) for the thermal degradation of the side chain (360°C) until the degradation was completed; finally, it was heated at 490°C (T_p for the thermal degradation of the main chain) until the degradation was completely finished. FTIR/TGA was performed on a combined PerkinElmer Spectrum Gx-I/TGA-7 system with real-time software. The pyrogenic decomposition gases of the prepared nanocomposite were transferred from the TGA analyzer to the FTIR/TGA interface and measured by FTIR spectroscopy with a 4-cm^{-1} resolution.

RESULTS AND DISCUSSION

Interactions of the nanocomposite

With the SAM method, the surfaces of negatively charged SiO_2 nanoparticles are covered by positively charged molecular chains of PAH through electrostatic adsorptive interactions (Fig. 1), which significantly improve the dispersion of SiO_2 nanoparticles. Acute aggregations exist if SiO_2 nanoparticles are dispersed in pure water without any treatment (Fig. 2). However, there are no obvious aggregations after SiO_2 nanoparticles are treated with PAH (Fig. 3). The amido functional groups of PAH, which covers the surface of SiO_2 nanoparticles, are linked to hydroxy-functional groups of PVA by hydrogen-bonding interactions, which result in the uniform dispersion of SiO_2 nanoparticles in the PVA matrix. The TEM micrograph of the prepared nanocomposite

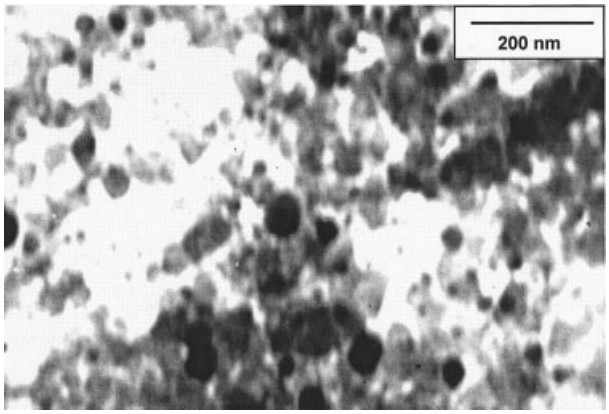

Figure 3 Micrograph of the dispersion of SiO_2 nanoparticles treated with PAH (TEM).

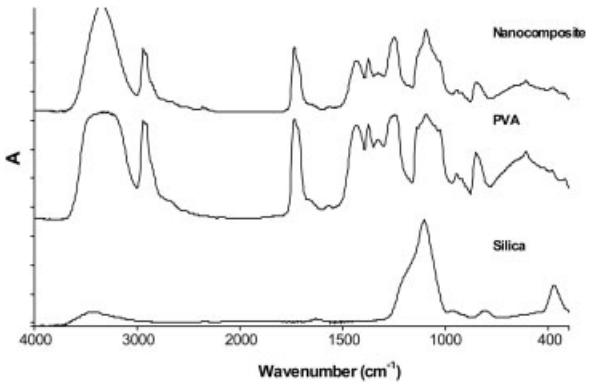

Figure 5 FTIR spectra of SiO_2, PVA, and the PVA/SiO_2 nanocomposite.

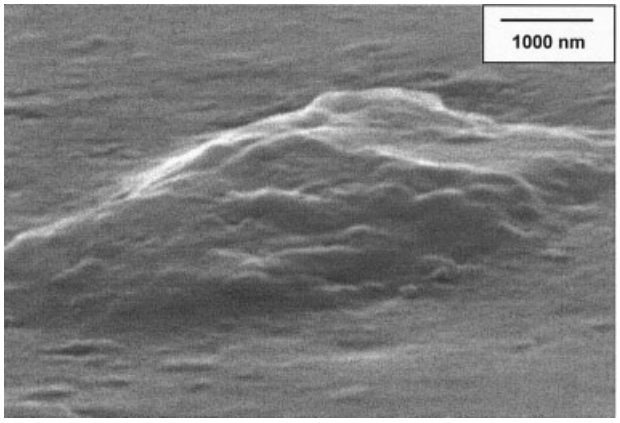

Figure 6 Micrograph of pure PVA (SEM).

shows that the SiO_2 nanoparticles do not aggregate in the PVA matrix (Fig. 4).

The interactions of the nanocomposite have also been investigated with FTIR. Figure 5 shows the plots of infrared spectra of the pure PVA, PVA/SiO_2 nanocomposite, and SiO_2 where A is defined as absorbance behind nanoparticles. The untreated PVA sample has a broad and strong band centered at 3306 cm^{-1}, which is assigned to the stretching vibration of hydroxy with strong intra-hydrogen bonding, whereas that of the PVA/SiO_2 nanocomposite is shifted to 3343 cm^{-1}, and its shape becomes narrow and acute. This may be due to the interaction between the SiO_2 nanoparticles and PVA matrix, which obstructs the formation of intra-hydrogen bonding. The characteristic absorbing peaks of SiO_2 (1100 and 466 cm^{-1}) are not simply overlapped by those of PVA but move to 1089 and 473 cm^{-1}, respectively. This further indicates that the PVA matrix and SiO_2 nanoparticles are not simply blended, and complex interactions exist.

Morphology of the nanocomposite

Figures 6 and 7 are SEM micrographs of the pure PVA and prepared nanocomposite, respectively. The roughness in Figure 7 is related to the presence of SiO_2 particles coated by the PVA matrix. There is no obvious SiO_2 aggregation in the PVA matrix, and the SiO_2 particles, ranging from 20 to 50 nm, are distributed in PVA matrices uniformly. This coincides with the TEM investigation (Fig. 4), which shows that the PVA matrix can be well assembled with SiO_2 nanoparticles through the formation of hydrogen bonds.

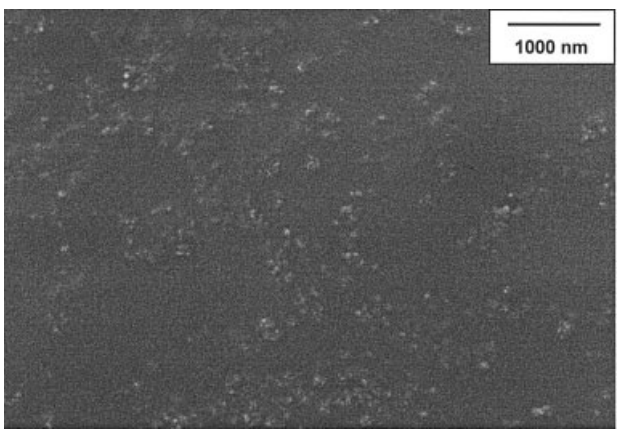

Figure 7 Morphology of the PVA/SiO_2 nanocomposite (SEM).

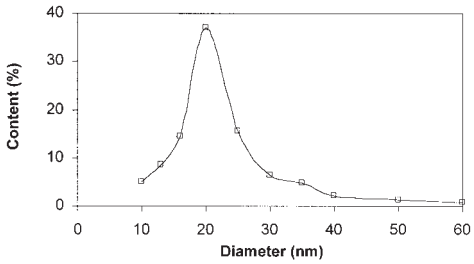

Figure 8 Size distribution of the SiO_2 phase in the PVA matrix.

From more than 300 particles in three different TEM micrographs, we have found that the SiO_2 particles are 10–60 nm in size, and 38% have a mean size of approximately 20 nm, which is the highest distribution (Fig. 8). In an image of elemental mapping for Si (Fig. 9), no large mineral aggregations can be seen, and the uniformity of the white dots indicates that there is no obvious agglomeration of SiO_2 nanoparticles. In comparison with the pure PVA (Fig. 6), the surface of the PVA/SiO_2 nanocomposite is smoother (Fig. 7). As PVA is a kind of semicrystalline polymer, quite a few crystallites are formed on the surface of the pure PVA fracture, whereas there are no crystallites on the surface of the PVA/SiO_2 nanocomposite because of the well-dispersed SiO_2 nanoparticles being able to prevent the formation of crystallites.

DSC analysis

There is a very similar trend for DSC curves of the pure PVA and PVA/SiO_2 nanocomposite (Fig. 10).

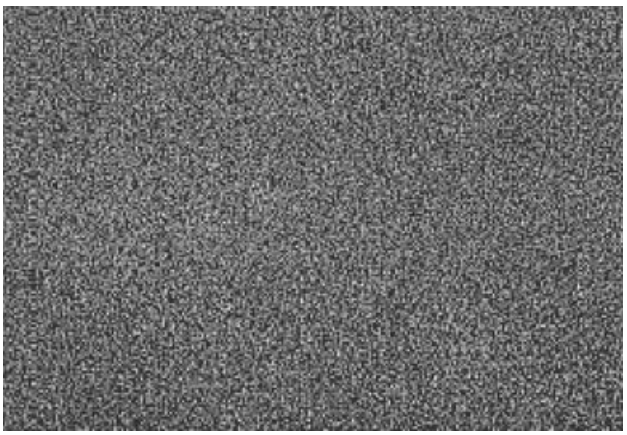

Figure 9 Si mapping photograph of the PVA/SiO_2 nanocomposite.

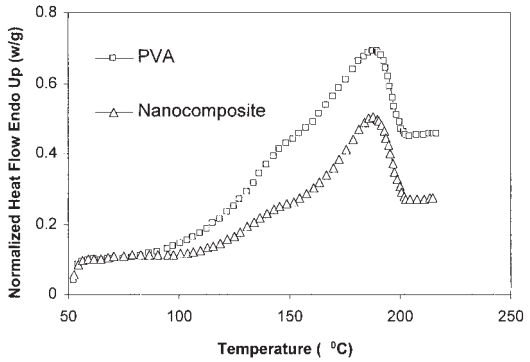

Figure 10 DSC curves of pure PVA and the PVA/SiO_2 nanocomposite.

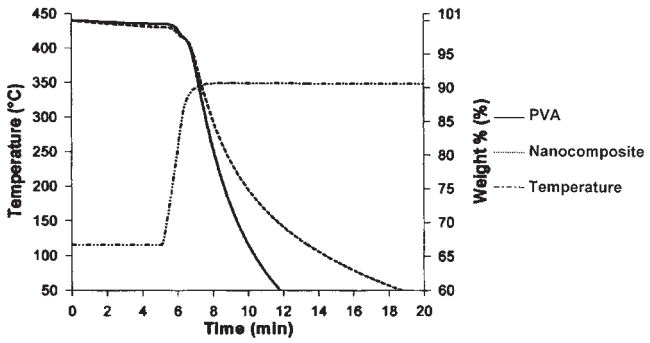

Figure 12 TGA curves and programming temperature versus the time.

The DSC curve of the prepared nanocomposite, in relation to that of the pure PVA, has been moved to a higher temperature within the range of T_g. T_g of the pure PVA is 121.2°C, whereas that of the prepared nanocomposite increases to 131.9°C. The addition of the SiO_2 nanoparticles to the PVA matrix results in a significant increase in T_g. This suggests that the SiO_2 nanoparticles are well dispersed in the PVA matrix. Because nanoparticles have huge relative surface areas and strong adsorptive power, the amorphous molecular chains of PVA become stable and interact strongly with the SiO_2 nanoparticles. As a result, the SiO_2 nanoparticles restrict the thermal motion of the PVA molecular segments. Because T_g is the limiting temperature for the applications of plastic polymers, an improvement in T_g is very important for PVA. As for T_m, there seems to be no clear change between the PVA and PVA/SiO_2 nanocomposite.

TGA

Figure 11 presents thermogravimetric/derivative thermogravimetric (TGA/DTG) curves of the pure PVA and PVA/SiO_2 nanocomposite in a nitrogen atmosphere at a heating rate of 20°C/min. The degradation curve of the prepared nanocomposite moves to a higher temperature in comparison with that of the pure PVA. T_p at the two degradation peaks for the nanocomposite increases 22.0 and 20.0°C, respectively, over those of the pure PVA. This demonstrates that the thermal resistance of the prepared nanocomposite is better than that of the pure PVA.

Figure 12 presents the isothermal TGA curves with the heating time for the pure PVA and prepared nanocomposite. Under the same heating conditions, PVA needs to be heated for 11.8 min, whereas the nanocomposite requires 18.6 min to reach the same degradation rate (40%). Therefore, the thermal decomposition of the nanocomposite is obviously delayed, and the thermal stability of the nanocomposite is significantly improved, in comparison with those of the pure PVA. The improved efficiency in the thermal stability of the nanocomposite may be due to the addition of SiO_2 nanoparticles within the PVA matrix. While being heated, the SiO_2 nanoparticles migrate to the surfaces of the composites, probably because they have a relatively low surface potential energy and SiO_2 on the surfaces of the composites therefore acts as a heating barrier to protect the PVA inside. This needs to be further studied with adequate measurements, such as X-ray diffraction analysis (XRD).

FTIR/TGA

There are two obvious peaks in the Gram–Schmidt chromatogram (Fig. 13). The peak between 5 and 15

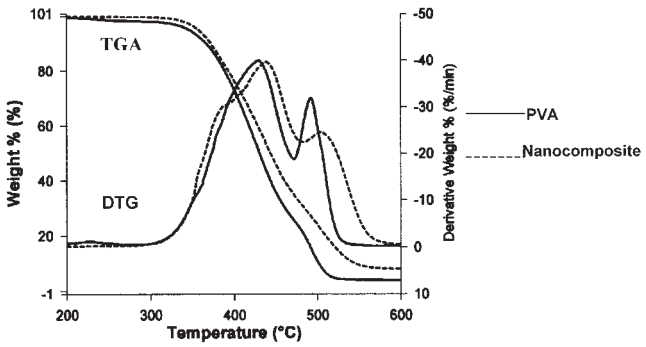

Figure 11 TGA/DTG curves of PVA and the PVA/SiO_2 nanocomposite.

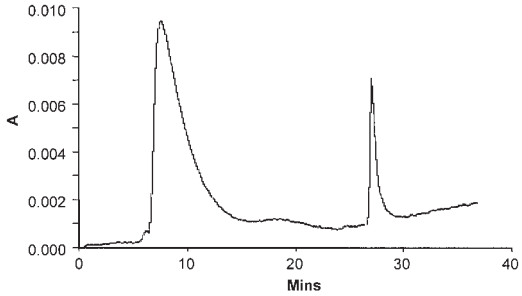

Figure 13 Gram–Schmidt chromatogram of the thermal degradation.

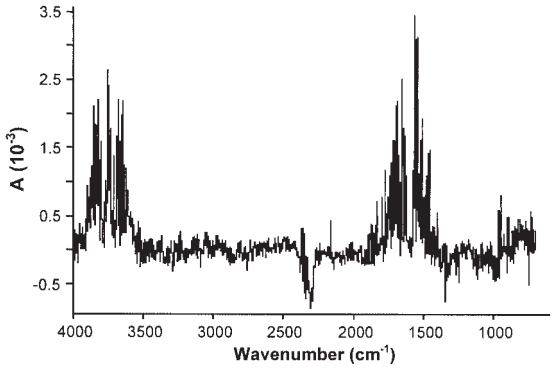

Figure 14 FTIR spectrum of the evolved water vapor.

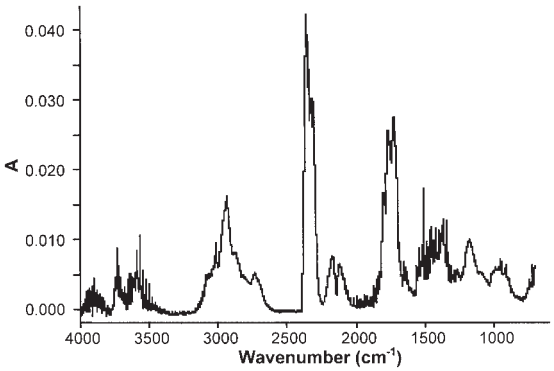

Figure 16 FTIR spectrum of the gases that evolved from main-chain degradation.

min corresponds to the gases evolving from the degradation of side chains, and the peak at 25–30 min can be attributed to the gases evolving from the degradation of main chains. The FTIR spectrum of the evolving gases from 0 to 5 min is a typical FTIR spectrum of water vapor (Fig. 14).

Figure 15 presents the FTIR spectrum of gases that evolved from decomposed side chains. As for liquid or solid carboxylic acid, the stretching vibration peak of C═O is at about 1710 cm^{-1} and is relatively wide. The wide stretching vibration peak of O—H normally occurs at 2500–3300 cm^{-1}. When carboxylic acid is gas, the stretching vibration peaks of O—H and C═O are shifted to 3560 and 1790 cm^{-1}, respectively, and become narrow and acute. This indicates that during thermal degradation, the side chains are decomposed, and carboxylic acid evolves.

Figure 16 presents the spectrum of the gases that evolved from disintegrated main chains. The evolved gases contained carbon dioxide, low-molecular-weight conjugated polyene at an absorbing peak (1650 cm^{-1}), and low-molecular-weight alkyne at a C≡C stretching vibration (2200–2050 cm^{-1}).

A three-dimensional FTIR spectrum (Fig. 17) shows that the thermal degradation of the PVA/SiO_2 nanocomposite has two steps. During the first stage, side chains decompose and carboxylic acid evolves as an effect of heating. As the degradation proceeds, side chains are completely decomposed, and the main chains disintegrate into carbon dioxide, low-molecular-weight alkyne, and conjugated polyene. In addition to the delay in the decomposition temperature, this degradation process is similar to that of the pure PVA. This means that the addition of the SiO_2 nanoparticles does not destroy the basic thermal degradation mechanism of PVA but improves its thermal stability.

CONCLUSIONS

A novel method for preparing a PVA/SiO_2 nanocomposite with the SAM technique has been presented. Although SiO_2 nanoparticles and PVA are immiscible, through a treatment with the SAM technique, the PVA matrix can come into close contact with treated SiO_2 nanoparticles through electrostatic adsorption and hydrogen bonding, and this results in the uniform dispersion of SiO_2 in the PVA matrix. The size of the SiO_2 phase in the PVA matrix is about 20 nm.

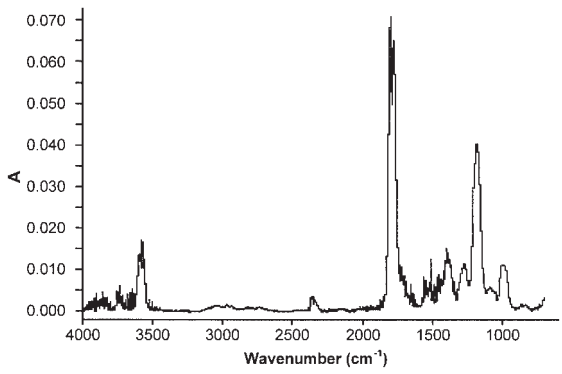

Figure 15 FTIR spectrum of the gases that evolved from side-chain degradation.

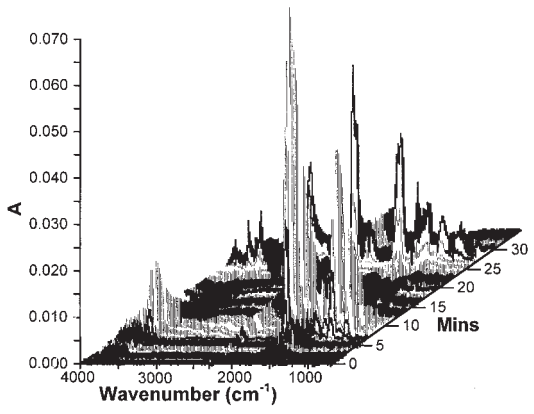

Figure 17 Three-dimensional FTIR spectrum of the thermal degradation.

The T_g values and the T_p values for the thermal degradation of side and main chains of the prepared nanocomposite increase 10.7, 22.0, and 20.0°C over those of the pure PVA, respectively. When the nanocomposite is isothermally heated, its decomposition is delayed markedly in comparison with that of the pure PVA. The thermal degradation of the nanocomposite is a two-step reaction. Carbon dioxide, low-molecular-weight alkyne, and conjugated polyene evolve from decomposed main chains after carboxylic acid is engendered from disintegrated side chains.

References

1. Supronowicz, P. R.; Ajayan, P. M.; Ullmann, K. R. J Biomed Mater Res 2002, 59, 499.
2. Zhang, R.; Ma, P. X. J Biomed Mater Res 2000, 52, 430.
3. Bauer, F.; Sauerland, V.; Gläsel, H. J. Macromol Mater Eng 2002, 287, 546.
4. Zyl, W. E. V.; García, M.; Schrauwen, B. A. G. Macromol Mater Eng 2002, 287, 106.
5. Jenekhe, S. A.; Yi, S. Adv Mater 2000, 12, 1274.
6. Solaro, R.; Corti, A.; Chiellii, E. Polym Adv Technol 2000, 11, 873.
7. Kim, S. Y.; Lee, Y. M. J Appl Polym Sci 1999, 74, 1752.
8. Shaheen, S. M.; Ukai, K.; Dai, L.; Yamaura, K. Polym Int 2002, 51, 1390.
9. Queiroz, A. A. A.; Ferraz, H. G.; Abraham, G. A. J Biomed Mater Res A 2003, 64, 147.
10. Wang, W. K.; Campbell, G.; Zhang, Z. F. J Biomed Mater Res 2002, 63, 854.
11. Carbone, K.; Casarci, M.; Varrone, M. J Appl Polym Sci 1999, 74, 1881.
12. Yoshioka, S.; Aso, Y.; Nakai, Y.; Kojima, S. J Pharm Sci 1998, 87, 147.
13. Rhim, J. W.; Yeom, C. K.; Kim, S. W. J Appl Polym Sci 1998, 68, 1717.
14. Rhim, J. W.; Kim, Y. K. J Appl Polym Sci 2000, 75, 1699.
15. Nakane, K.; Yamashita, T.; Iwakuka, K.; Suzuki, F. J Appl Polym Sci 1999, 74, 133.
16. Lin, H.; Watanabe, Y.; Kimura, M. J Appl Polym Sci 2003, 87, 1239.
17. Ione, C.; Daniel, L.; Angel, A.; Carmen, M. J Polym Sci Part B: Polym Phys 2001, 39, 1968.
18. Decher, G.; Hong, J. D. Makromol Chem Macromol Symp 1991, 46, 321.
19. Kotov, N. A. Nanostruct Mater 1999, 12, 789.
20. Shimazaki, Y.; Mitsuish, M.; Ito, S. Langmuir 1999, 32, 8220.
21. Hao, C.; Wang, L.; Zhang, J. Chem Lett 1999, 5.
22. Kim, J.; Wang, H.; Kumar, J. Chem Mater 1999, 11, 2250.
23. Williams, L. M.; Evans, S. D.; Marsh, T. M. Langmuir 1997, 13, 751.
24. Lvov, Y. M.; Rusling, J. F.; Thomsen, D. L. Chem Commun 1998, 1229.
25. Ariga, K.; Lvov, Y.; Onda, M. Chem Lett 1997, 125.